energies

MDPI

Article

Wireless Power Transfer Technology Applied to an Autonomous Electric UAV with a Small Secondary Coil

Tommaso Campi *, Silvano Cruciani and Mauro Feliziani

Department of Industrial and Information Engineering and Economics, University of L'Aquila, 67100 L'Aquila, Italy; silvano.cruciani@univaq.it (S.C.); mauro.feliziani@univaq.it (M.F.)
* Correspondence: tommaso.campi8888@gmail.com; Tel.: +39-086-243-4421

Received: 11 January 2018; Accepted: 30 January 2018; Published: 2 February 2018

Abstract: This study deals with the design and the optimization of a wireless power transfer (WPT) charging system based on magnetic resonant coupling applied to an electric vertical take-off and landing Unmanned Aerial Vehicle (UAV). In this study, a procedure for primary and secondary coil design is proposed. The primary circuit in the ground station consists of an array of coils in order to mitigate the negative effects on the coupling factor produced by the possible misalignment between the coils due to an imperfect landing. Key aspects for the design of the secondary coil onboard the UAV are the lightness and compactness of the WPT system components. A demonstrative prototype of the WPT system is applied to a commercial drone. The WPT electrical performances are calculated and measured. Finally, an automatic battery recharge station is built where the drone can autonomously land, recharge the battery and take off to continue its flight mission.

Keywords: magnetic resonant coupling; wireless power transfer (WPT); drone; Unmanned Aerial Vehicle (UAV); automated battery recharge station; magnetic field

1. Introduction

The use of lightweight electric vertical take-off and landing Unmanned Aerial Vehicles (UAVs) is becoming increasingly popular in various application areas such as surveillance, monitoring and couriers [1]. The UAVs can be equipped with many payloads such as a high resolution camera, infrared camera, sensors, etc., or with objects to deliver [2]. In general, these commercially available systems are powered by a high energy density lithium battery that permits a flight time of about 20–40 min [3,4]. This is one of the major limitations of these systems, especially in applications where a stand-alone operation of the UAV is required. In order to increase the flight time, one can substantially proceed in three ways. The first method consists of equipping the UAV with a higher battery capacity, but this inevitably results in an increased weight with a consequent reduction of the payload. A second alternative is to create a base station where the batteries can be automatically swapped immediately after landing [5]. This solution allows the UAV to take off in a very short time, but it could be impractical due to cost and complexity of these systems with many mechanical elements. The last alternative is to create base stations where the UAV lands to automatically recharge its battery. There are mainly two ways to realize a charging station: the first one is based on electrical contacts between the base station and the drone [6]. The second solution is based on the wireless power transfer (WPT) technology [7–13]. The contact-based solution allows high power transfer efficiency but the presence of contacts exposed to atmospheric agents will reduce the efficiency and reliability of the system. On the other hand, the WPT technology permits a very efficient and reliable power transmission between the ground base and the UAV. The application of this technology to UAV must take into account several aspects. The on-board WPT systems must be very lightweight to avoid

significant reduction of the payload (in general between 0.5 kg and 10 kg depending on the size of the lightweight UAV) [4]. Furthermore, the WPT systems must not interfere with the electronic systems of the UAV and with the communications between UAV and ground systems.

Finally, the WPT technology must guarantee efficient power transfer with high tolerance to coil misalignment, as is so often the case due to poor landing precision. The major issues to recharge drone batteries by WPT systems are described in several past works [14–19]. In [14], two circular planar spiral coils have been used for both primary and secondary circuits of a WPT system, the main disadvantages of this configuration are the significant weight and dimension of the on-board components that reduce the payload of the drone. In [15], an automatic landing procedure is presented to improve the landing precision reducing the possibility of misalignment condition between the transmitting and the receiving coils. A WPT charging system based on a mobile primary coil was presented in [16]. This system is based on a mechanic system to align the primary coil with the on-board secondary coil after landing. The main disadvantage is the complexity of the positioning system that could lead to reliability issues. Finally, a charging system based on radio frequency (RF) transmission was presented in [17]. This solution allows to improve the distance between transmitter and receiver but with a significant reduction of the efficiency and transferred power. Here, a significant improvement in the coil design is proposed with the goal of becoming less sensitive to the misalignment of the coils. The proposed solution consists in the design of a charging ground pad with multiple primary coils, i.e., an array of independent coils. The secondary coil, placed on-board the drone, must be very light. To this aim, a new WPT charging system has been designed, manufactured, installed and tested in a commercial drone focusing on the minimization of the weight, size and magnetic field emission, while maintaining good electrical performances in power transfer.

2. System Configuration

The main goal of a WPT system for a drone is to automatically recharge its battery. In the proposed application, the primary (or transmitting *Tx*) WPT coil is suitably selected from an array of independent planar coils placed in a ground pad station, while the secondary (or receiving *Rx*) planar coil is placed on-board the drone. Generally, drones are equipped with systems like high-definition cameras, infrared cameras, proximity sensors, etc. All these apparatuses need a viewing area that must not be disturbed by the WPT system (mainly the secondary coil) (see Figure 1). To meet this requirement, the first constraint in the WPT design concerns the shape and the size of the on-board secondary coil that must be adequately designed. At the same time, the WPT charging system must be reasonably efficient in terms of electrical energy and transferred power. Typically, a drone battery is composed by 3 to 6 Li-Po cells that correspond to a battery voltage between 11.1 V and 22.2 V, with a capacity between 3 Ah and 10 Ah [4]. This type of battery can be recharged in approximately one hour. The fast charging procedure requires that a significant amount of power must be transmitted to the drone.

In a previous work [14], the on-board coil has been placed under the drone frame. Such a solution permits the installation of the coil without interfering with the payload, but the air gap between the ground and the on-board coil is relevant (typically much more than 100 mm). Adopting this configuration, it is necessary to use large coils and some ferrite to obtain high levels of WPT efficiency leading to a significant increase of the on-board components weight. In the proposed new configuration, the receiving coil is placed on the landing skid reducing dramatically the vertical air gap between the transmitting and the receiving coils. This solution permits a large enhancement of the system performance due to the increase of the coupling factor between the coils. The use of ferrite is therefore not necessary. Thus, it is possible to design a very small and lightweight secondary coil maintaining high power transmission efficiency. For the considered landing skid, a narrow rectangular shape of the secondary coil is selected. This shape of the secondary coil, even if it is not the best solution for inductive coupling and energy transfer, fits very well with the skid and does not compromise the aerodynamics and the viewing area of the cameras. Another advantage is the position of the secondary coil, which is far from the drone frame where the electronic components are located. This reduces

considerably the risk of electromagnetic interference on the electronic systems of the drone due to the time varying magnetic field generated by the coil currents.

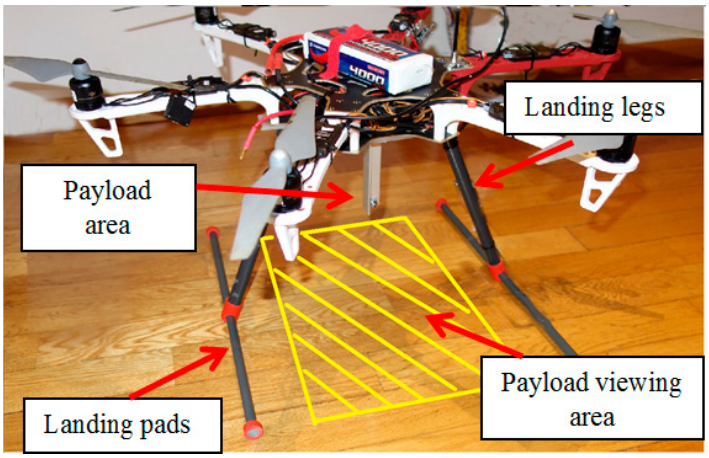

Figure 1. Typical drone landing support.

The main disadvantage of this configuration is the poor robustness to the misalignment condition due the small dimension of the secondary coil. This aspect is critical in drone applications where the landing precision could be poor since it depends on the accuracy of the landing assistance system. One solution can be the use of a primary coil much larger than the secondary coil, but this could lead to a low WPT efficiency due to a high leakage of the magnetic flux.

In this study, a high level of tolerance to misalignment condition is achieved adopting a multiple primary coils configuration, as reported in Figure 2, and it is composed by an array of independent primary coils placed suitably to entirely cover the charging area.

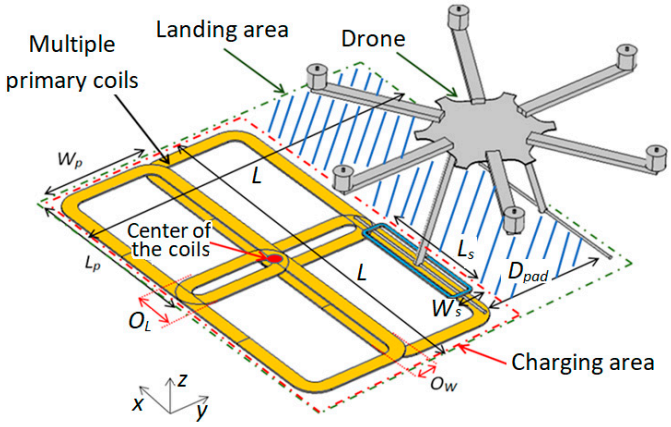

Figure 2. Configuration of the WPT charging coils for a drone.

The design of the primary coils is of paramount importance to ensure an adequate coupling with the secondary coil in all possible landing positions reducing the total number of coils in the array. When the drone is landed, an automatic procedure starts to determine which coils in the landing area presents the maximum coupling with the secondary coil. Then, this coil is the only one selected to charge the battery. The optimization of the primary coils shape and dimension permits to reduce the number of coils on the charging pad reducing complexity and cost.

The electronic configuration is optimized to reduce the weight of the on-board components. In a typical WPT charging system, the regulation of the battery charging is performed on the receiving

side before the battery. Here, to save on-board weight and space, the regulation is performed on the transmitting side. The adopted electrical configuration is reported in Figure 3. On the transmitting side, the DC voltage is regulated before the inverter using a DC-DC converter that permits the adjustment of the charging power. On the receiving side, the AC voltage from the coil and the compensation capacitors is rectified and directly connected to the battery. A wireless communication is used to establish a feedback between the battery and the charging regulator. Using this configuration, the only on-board components placed on the drone are the secondary coil, the compensation capacitors, the rectifier and the communication module.

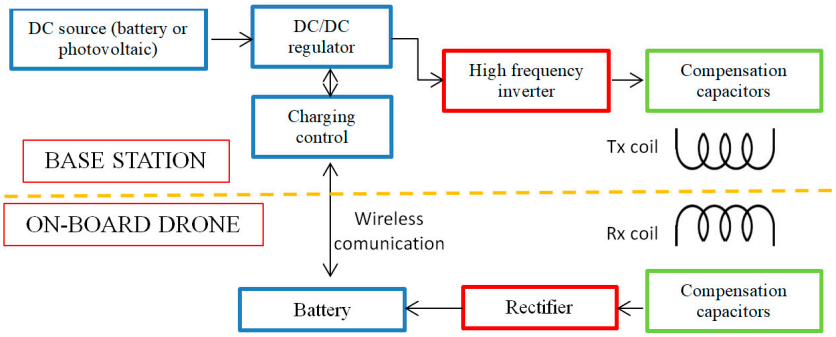

Figure 3. Adopted electrical configuration of the WPT charging for a drone.

3. WPT Design

3.1. WPT Equivalent Circuit

The WPT technology allows to transfer electrical energy by means of magnetic resonant coupling between two coils that act as a loosely coupled transformer. The complete electrical circuit of a WPT system is reported in Figure 4. The two coupled coils are characterized by self-inductances L_1 and L_2, mutual inductance M and self-resistances R_1 and R_2 that model the losses in the coils [20]. To reduce the AC losses due to skin and proximity effects the coils are made by a copper Litz wire. The coupling factor k is given by:

$$k = \frac{M}{\sqrt{L_1 L_2}} \tag{1}$$

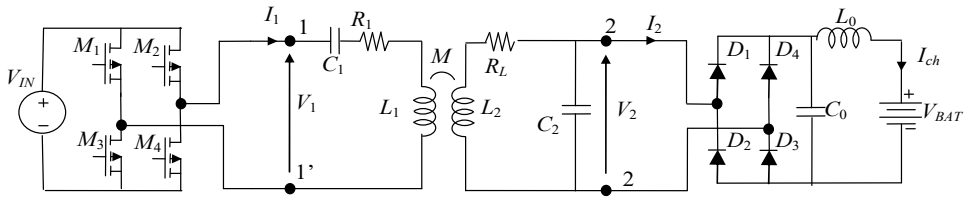

Figure 4. Electrical circuit of a WPT charging system with Series-Parallel (SP) compensation.

Capacitance compensation networks are added on transmitting and receiving sides to obtain resonance condition [21] and to improve the electrical performances of the system. There are several compensation network configurations that can be used in a WPT system. The most commonly used are the capacitive Series-Series (SS) and Series-Parallel (SP) topologies.

In real applications, the source and the load are composed by complex electronic blocks. At the transmitting side, a full bridge inverter made by MOSFETs (M_1, M_2, M_3, M_4) is adopted to generate a high frequency square wave voltage V_1 from the DC source V_{IN}. At the receiving side the high frequency voltage is firstly rectified by a full bridge rectifier, composed by diodes D_1, D_2, D_3, D_4. The DC output voltage is filtered by a low pass filter composed by a shunt capacitance C_0 and a series

inductance L_0. Finally, it is connected to the battery. However, to extract the lumped parameters of the system, a simplified circuit is adopted as shown in Figure 5. The primary circuit can be modeled by a simple sinusoidal voltage source V_g with a very small internal resistance R_g. In addition, the load can be simplified and modeled by an equivalent resistance R_L [9].

The lumped inductances (L_1, L_2 and M) are numerically extracted at the frequency of interest solving the magneto quasi-static (MQS) field equations by the commercial software COMSOL [22], while the AC resistance of the Litz wire is obtained from wire datasheet [23]. After the evaluation of the circuit lumped parameters, the compensation capacitors C_1 and C_2 can be obtained at the given resonance frequency for the selected compensation topology [20]. The resonant frequency of 150 kHz [14] is here adopted for this kind of application since it is commonly used for the medium power application (e.g., mobile device). This frequency allows the transfer of an adequate amount of power with good efficiency at short range.

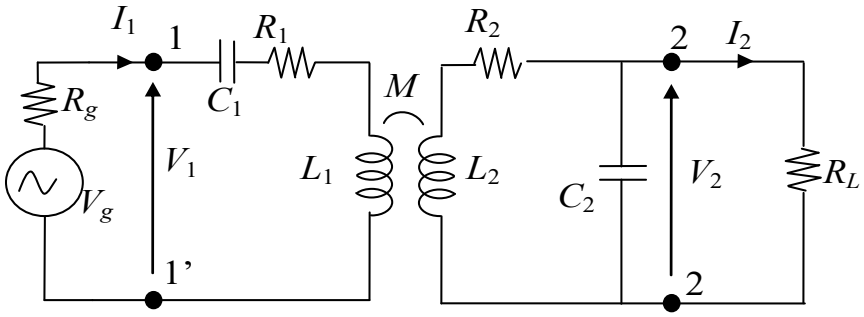

Figure 5. Simplified equivalent circuit of two coupled coils with SP compensation.

Higher operational frequency should permit an improvement of the power transfer, but it could require a more complex electronic system and could generate electromagnetic interference (EMI) issues [24,25].

The electrical performances of the WPT system, i.e., efficiency and transferred power, are obtained by the analysis of the equivalent simplified circuit. The transferred power $P_L = R_L |I_2|^2$ is the power dissipated on the load resistance R_L, while the efficiency $\eta = P_L/P_1$ is calculated as the ratio between the output real power P_L and the input real power at port 1-1′ [20].

In order to choose the configuration with the best weight to performance ratio, a comparison between SS and SP compensation topologies is carried out. Two planar stacked coils of rectangular shaped are considered. The *Tx* coil has outer dimensions L_p = 400 mm, W_p = 150 mm while the *Rx* coil has outer dimensions L_s = 20 mm, W_s = 50 mm. The intraturn spacing is negligible. The separation distance between parallel coils is fixed at D = 10 mm. The Litz wire used for both *Tx* and *Rx* coils has an external diameter of d_{wire} = 3 mm. The load is modeled by a resistor R_L = 3 Ω. The efficiency is then calculated for the two examined compensation topologies (SS and SP) varying the number of turns, N_1 and N_2, of the *Tx* and *Rx* coils, respectively, while keeping fixed the outer dimensions of the coils. The obtained results, reported in Figure 6, show that the maximum efficiency of the SP compensation is similar to that of the SS compensation when assuming N_1 = 8, but with a different number of turns of the secondary coil. For the SP configuration, the maximum efficiency is obtained for N_2 = 2 while for the SS compensation it is obtained for N_2 = 8. It is therefore evident the great advantage of the SP compensation topology in respect of the SS compensation topology for the minor number of the secondary turns.

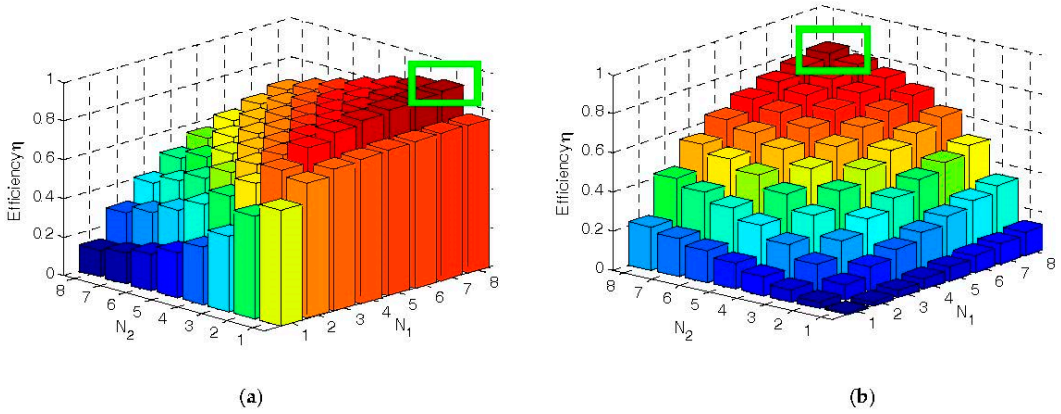

Figure 6. Efficiency vs. number of turns N_1 and N_2 considering SP topology (**a**) and Series-Series (SS) topology (**b**).

This configuration leads also to a considerable weight reduction of the on-board components. The efficiency and weight of the secondary coil vs. N_2 for N_1 = 8 are shown in Figure 7 demonstrating that the SP compensation is better than the SS compensation for the considered application. Thus, the SP compensation topology is adopted and applied to a WPT system for a commercial drone, as described in the following.

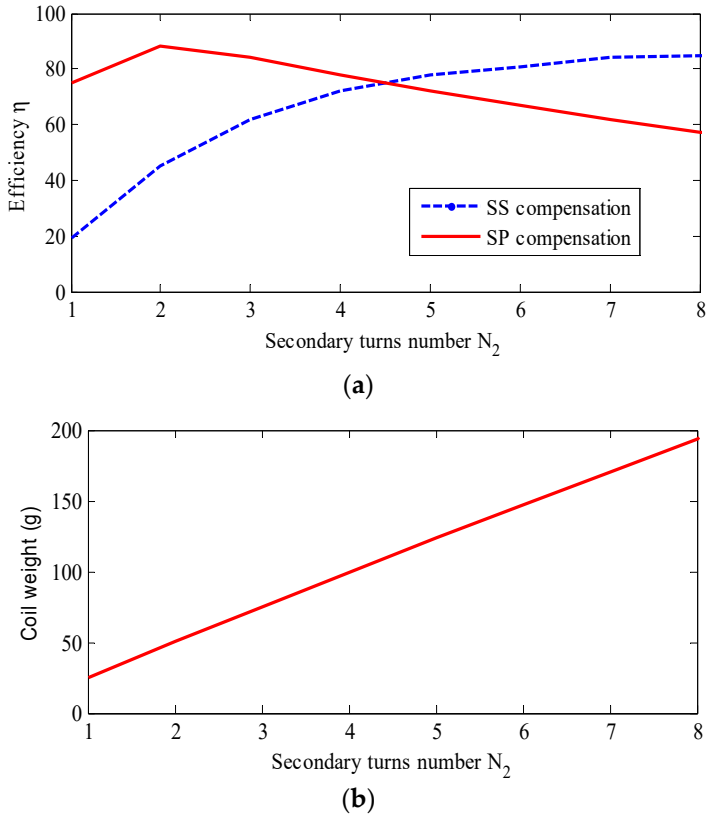

Figure 7. Efficiency η vs. number of turns N_2 when N_1 = 8 considering SP and SS topologies (**a**). Secondary coil weight vs. number of turns N_2 (**b**).

3.2. Coil Design

The goal of the primary coil array design is to ensure an adequate efficiency of the WPT system at any point in the landing area, and at the same time to minimize the number of the independent

primary coils in the array. It means that the WPT system efficiency η must be greater than a preset value η_{min} at any point of the ground pad where the drone can land. The dimensions and number of the primary coils are obtained by the procedure schematized in Figure 8. The procedure starts by fixing the system requirements in terms of electrical and geometrical constraints. The electrical constraints are the output voltage and power, and the resonant frequency. The geometrical constraints are the dimensions, the shape and the weight of the on-board secondary coil (they are set in advance to fit the landing pad, to guarantee mechanical robustness and aerodynamics, and to avoid any obstruction to the vision of on-board sensors or cameras). Another geometrical constraint is the size of the square landing area with side length L where the array of primary coils is installed.

The secondary coil of small size and narrow rectangular shape is placed on one skid of the landing gear. Since the autopilot of the drone can ensure a near perfect angular alignment during the landing, it is possible to orient the drone in such way that the landing skids are always parallel to one long side of the square landing pad.

The battery charging area is smaller than the landing area. Indeed, the small receiving coil will never be positioned in the area covered by the drone (i.e., area between the two skids and depicted as dotted blue area in Figure 2), otherwise part of the landing gear should be outside the landing area and this is clearly not acceptable. In conclusion, the charging area has a size smaller than the landing area and the narrow rectangular secondary coil is always well oriented. The variables of the optimization procedure are the primary coil dimensions W_p and L_p, the overlapping distance between adjacent coils O_W and O_L, and the array dimension N_{Cx} and N_{Cy} of the primary coils. The rectangular primary coils are assumed to be identical to each other. The ratio of the coil sides L_p/W_p is kept fixed to permit an adequate coupling with the secondary coil. In addition, the ratio O_L/O_W and the number of turns N_1 and N_2 are considered fixed. Only the misalignments along the x- and y-directions are variable in the proposed application, while the vertical separation of the coils along z (i.e., air gap) is kept fixed. It should be noted that the intraturn spacing could also be a design variable. However, for the considered frequency, the gain in terms of efficiency varying the spacing is very small due to the use of Litz wire, thus for the sake of simplicity it is considered fixed in this procedure [9].

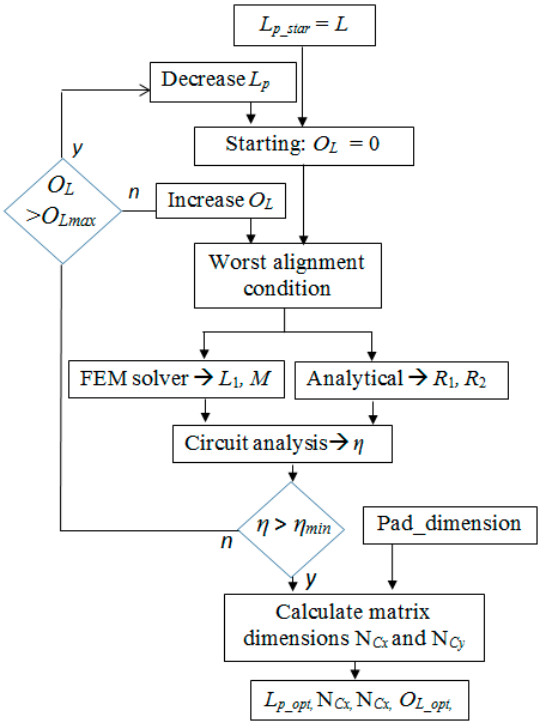

Figure 8. Flow chart of the coil design procedure.

The WPT efficiency η is calculated for any possible landing point by the analysis of the equivalent circuit, whose lumped parameters are extracted numerically for any mutual position between primary and secondary coils [26]. The algorithm is based on the iterative reduction of the single primary coil dimensions and the increase of the overlapping distance. Smaller dimensions of the primary coils permit to reduce the flux leakage improving the coupling factor with the secondary coil (and then the efficiency). The optimization of the overlapping distances O_L and O_W is important to obtain an efficiency $\eta > \eta_{min}$ also at the points where two or more coils are overlapped.

The procedure starts considering as initial parameters:

- Resonance frequency f.
- Coil side L_p equal to the side L of the landing area.
- Overlapping $O_L = 0$.

If the calculated minimum efficiency is lower than a preset value, $\eta > \eta_{min}$, the overlapping distance O_L is increased and the procedure is iterated. If it reaches the maximum possible value O_{Lmax} ($O_L > O_{Lmax}$), the algorithm restarts decreasing the coil dimension L_p. The procedure is repeated until the calculated efficiency is higher than η_{min} at any point inside the charging area. At the end of the procedure the optimum primary coil dimensions L_{p_opt} and W_{p_opt}. are obtained, as well as the optimum overlapping factors O_{L_opt} and O_{W_opt}. The numbers of the primary coils N_{Cx} in x-direction and N_{Cy} in y- direction are finally calculated to entirely cover the charging area by:

$$N_{Cx} = \left\lfloor \frac{L - O_W}{W_{p\_opt} - O_{W\_opt}} \right\rfloor + 1 \quad (2)$$

$$N_{Cy} = \left\lfloor \frac{L - O_L}{L_{p\_opt} - O_{L\_opt}} \right\rfloor + 1 \quad (3)$$

where $\lfloor \rfloor$ represents the greatest integer floor. Thus, the overall dimensions of the landing pad are found as as $(L_{p\_opt} - O_{L\_opt})\, N_{Cx} \times (W_{p\_opt} - O_{W\_opt})\, N_{Cy}$ If this size is much larger than the preset value $L \times L$, all the dimensions can be resized, otherwise they remain unaltered.

4. Applications

4.1. Coil Design

In our calculations, the geometry and shape of the secondary coil are chosen to fit the landing pad, that results in a rectangular shape with side dimensions $L_s = 220$ mm and $W_s = 45$ mm. The number of the coil turns is selected following the procedure described in Section 3.2 resulting as $N_1 = 8$ and $N_2 = 2$. The vertical separation between the pad and the receiving coil is fixed to $D = 10$ mm. The landing area dimensions depend on the expected precision of the autonomous landing system [27]. For this application a side $L = 700$ mm is considered at the beginning of the iterative procedure for the square landing area. As described in the previous section, the charging area is smaller than the landing area. Considering a distance between the two landing skids $D_{pad} = 400$ mm the charging area has dimension $L_x = L - D_{pad} = 300$ mm and $L_y = L = 700$ mm. The ratio between the sides of the primary coil L_p/W_p and the overlapping distance O_L/O_W is set equal to 2.5 to obtain an adequate coupling with the secondary coil of narrow rectangular shape. The minimum efficiency is set to $\eta_{min} = 75\%$. The optimized results at the end of the iterative procedure are:

- Primary coil dimension $L_{p\_opt} = 375$ mm.
- Array size $N_{Cx} \times N_{Cy}$ with $N_{Cx} = 2$ and $N_{Cy} = 2$.
- Overlapping distance $O_{L\_opt} = 50$ mm.
- Side of the square landing area $L = 700$ mm.

The array of independent primary coils is therefore designed with the dimensions described above.

Once the drone is landed, a procedure starts to detect which coil of the array must be activated. The selection of the primary coil is based on the analysis of the input impedance Z_{in} at the primary port 1-1′ of the WPT circuit [28]. The input impedance is calculated as the ration between voltage and the current before the compensation network. The impedance Z_{in} is maximum when the coupling factor k is maximum, as shown in Figure 9. To find the primary coil showing the best coupling factor (and then the best efficiency) with the on-board secondary coil, each of the n Tx coil is individually connected by the control unit (CU) to the compensation network through electronics switches S_1, S_2, . . . , S_i, . . . , S_n as shown in Figure 10, and the resulting impedance $Z_{in,i}$ of the ith coil is stored. At the end of the procedure the CU compares the stored n values of the input impedance and select the Tx coil showing the maximum value of the input impedance, $Z_{in,max}$, to be used for the WPT charging process.

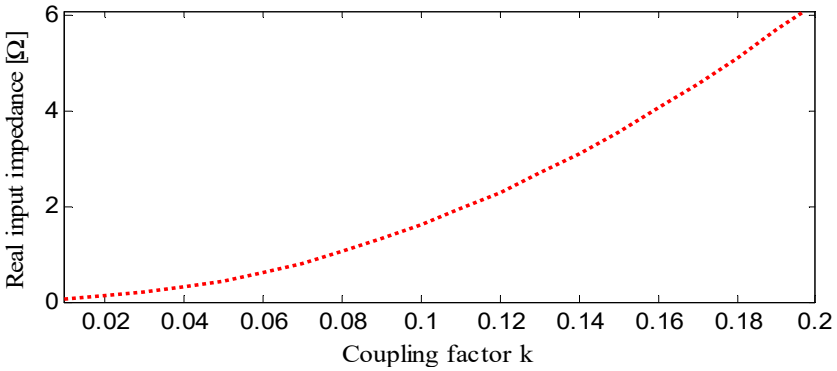

Figure 9. Input impedance vs. coupling factor k.

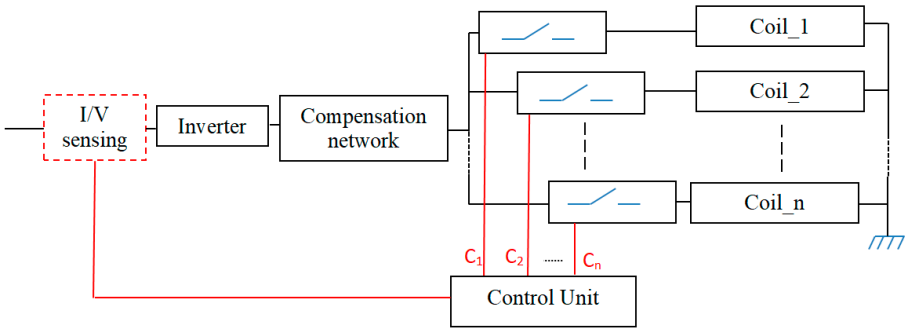

Figure 10. Transmitting coils connection scheme.

4.2. Numerical Results

The commercial drone DJI F550 (DJI, Shenzhen, China) is considered. It is characterized by a battery pack composed of 4 lithium cells with a capacity of 4 Ah. The goal is to recharge the battery in about one hour, that implies a DC current I_{bat} = 4 A. Considering the fully charged voltage V_{max} = 16 V the required power for the WPT system is P_L = 64 W. Then, the necessary electrical parameters are:

- Output voltage V_{bat} = 16 V.
- Output current I_{bat} = 4 A.
- Output power P_L = 64 W.

The battery is modeled by an equivalent resistance R_{eq}:

$$R_{eq} = \frac{V_{bat}}{I_{bat}} \tag{4}$$

which is set to $R_{eq} = 4\ \Omega$. The equivalent load resistance that models the full bridge inverter and the filter is calculated as $R_L = 0.81R_{eq}$, obtaining $R_L = 3.24\ \Omega$ [29]. In real applications, the load resistance R_L varies according to the status of the battery charge, but this variation is very limited and then a fixed value of R_L can be a valid assumption [30].

The efficiency is calculated in the considered charging area of 700×300 mm^2 size (assuming a 700×700 mm^2 landing pad and a separation of 400 mm between the two landing skids) for three different test cases to highlight the importance of the coil design procedure. In the first case, the charging area is entirely covered by a unique large coil. In the second case, the charging area is covered by an array of coils with the proposed dimensions but without overlapping between the coils ($O_L = O_W = 0$). In the third case, the primary coils array with optimized parameters derived by the proposed method is considered. The efficiency maps for the three test cases are reported in Figure 11. The efficiency is calculated in a grid of landing points inside the charging area. A landing point is assumed to be coincident with the projection of the secondary coil central point on the ground. In the first case, with only one large primary coil the efficiency is very poor in the whole area due to a big flux leakage caused by very different dimensions of the *Tx* and *Rx* coils. In the second case, the efficiency is good inside the four coil surfaces but there are some areas on the coil boundaries where the efficiency is dramatically reduced. Finally, in the third case, coincident with the proposed solution, the efficiency target $\eta > 75\%$ is widely respected at any landing point of the charging area due to the coil overlapping.

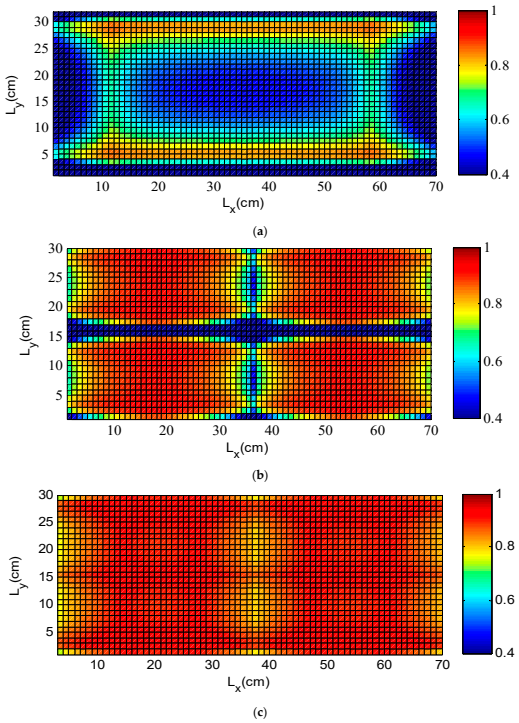

Figure 11. Calculated efficiency on the charging area for one primary coil (**a**), four primary coils without overlapping (**b**) and four primary coils with overlapping (**c**).

4.3. Electrical Performance

A WPT charging demonstrator based on the electrical and geometrical specifications reported in Section 4.1 has been realized and applied to a DJI F550 drone (see Figure 12a). The first tests were performed to validate the numerical results presented in the previous section in terms of electrical performances. A simplified electrical setup was therefore considered. The primary coil was fed by a half bridge inverter that allows adjusting the frequency and the amplitude of the modulated signal [18].

The receiving coil was connected to the load modeled as a simple power resistor R_L. As a first step, a RLC meter Keysight E4980A (Keysight, Santa Rosa, CA, USA) was used to measure the self and mutual inductances and resistances of the two stacked planar coils. The measured values are compared with the numerical results obtained by a FEM analysis (simulation setup is shown in Figure 12b) as reported in Table 1. Then, a comparison in terms of efficiency has been carried out fixing the output power to P_L = 64 W for three different *Rx* coil alignments. In the first case, the coils were perfectly aligned, while in the second and third cases the secondary coil was laterally misaligned in respect of the primary coil on the *x*-axis direction of 100 and 200 mm, and on the *y*-axis direction of 35 and 70 mm.

Table 1. Measured and calculated parameters of the WPT equivalent circuit parameters.

Method	R_1 (mΩ)	R_2 (mΩ)	L_1 (μH)	L_2 (μH)	M (μH)
Numerical	-	-	44.1	1.23	0.91
Measured	180	20	46.2	1.33	1.05

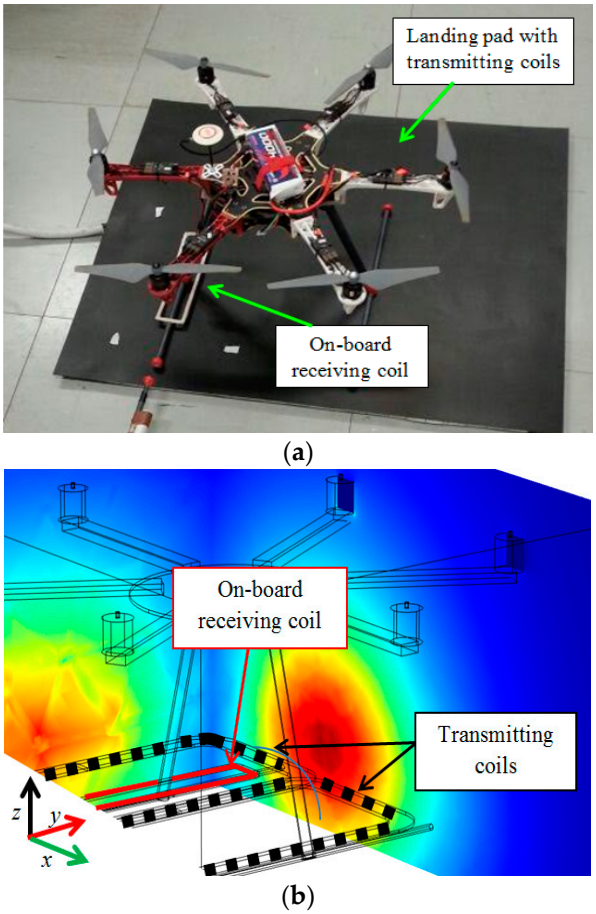

Figure 12. 3D model of the drone with WPT system for numerical simulation (**a**), demonstrator of the WPT system applied to a DJI F550 drone (**b**).

The input real power P_1 was derived measuring voltage, current and phase difference at the circuit port 1-1′ by an oscilloscope and a current probe, while the output power $P_L = |V_2|^2/R_L$ was derived measuring the voltage drop V_2 on the load resistance. In all the considered cases, the output power was kept fixed to P_L = 64 W adjusting the input voltage V_1. The electrical performances are measured and calculated for several misalignment conditions on the *x*-axis T_x and on the *y*-axis T_y. The obtained results reported in Table 2 show a good agreement between calculations and measurements.

Table 2. Measured and calculated electrical quantities of the WPT system circuit when P_L = 64 W.

Misalignment		Type	V_1 (V)	I_1 (A)	η (%)	P_1 (W)
T_x (mm)	T_y (mm)					
0	0	Calculated	11.7	6.2	88	72.5
		Measured	12.5	6	85	75
100	0	Calculated	10.2	7.6	83	77.5
		Measured	10.8	7.3	81	78.8
200	0	Calculated	8.5	9.6	78	81.6
		Measured	9.9	8.5	76	84.1
0	35	Calculated	12.0	6	89	71.9
		Measured	12.6	5.9	87	73.5
0	70	Calculated	12.3	5.8	90	71.1
		Measured	12.8	5.6	89	71.2

In the second test, all the real electronics components of the system are considered (see again the scheme in Figure 3) and applied on-board the drone as reported in Figure 12a. On the drone *Rx* side, the equivalent resistive load has been replaced with the rectifier [31] and the battery. The rectifier is composed by 4 ultra-low forward voltage Schottky diodes and has been placed with the compensation capacitors on the landing gear as shown in Figure 13. The efficiency of the complete system η_{tot} is then measured as the ratio between the power on the battery P_{bat} given by the product of the charging current I_{ch} and the battery voltage V_{bat} and power generated by the DC source P_{dc}. The obtained results are reported in Table 3, considering three different charging statuses of the battery, from fully discharged to fully charged for a misalignment on the *x*-axis T_x = 100 mm and on the *y*-axis of T_y = 40 mm.

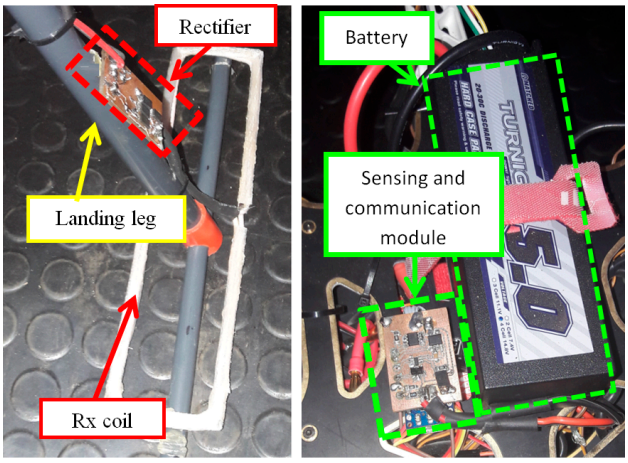

Figure 13. WPT charging system electronics on-board the drone.

Table 3. Measured electrical performances of the WPT system for three charging statuses of the battery and T_x = 100 mm T_y = 40 mm.

Battery Status (%)	V_{bat} (V)	I_{ch} (A)	P_{bat} (W)	P_{dc} (W)	η_{tot} (%)
10	12.8	4.1	52.4	64.7	79
50	14.4	4.0	57.6	72.9	78
100	16.4	4.0	65.5	85.2	76

The sensing circuit embeds a voltage probe, a current probe and a microcontroller to handle the communication with the base station. On the transmitting side, a DC/DC converter has been connected before the inverter and it is controlled by the CU. The CU processes the battery data from the drone and controls the charging procedure varying the setting of the converter. For this kind of battery, a constant-current/constant-voltage charging procedure is necessary.

Several operative tests have been performed verifying the validity of the proposed method. The charging of the battery is completed in about one hour after the automatic landing of the drone. Furthermore, it has been verified that the presence of the on-board *Rx* coil with electronics does not alter the flight capability of the drone, due to the very limited weight of the on-board WPT systems. In addition, the magnetic field emissions do not interfere with the drone Electronic Control Unit (ECU) and communication systems.

5. Conclusions

A WPT system is applied to an electric vertical take-off and landing UAV. All on-board components have been designed to be very light and compact in order to reduce weight and size as much as possible. By the design procedure, a small secondary coil with only two turns has been proposed and installed on a drone landing skid. This installation with a small air gap between primary and secondary coils leads to a high efficiency of the WPT system. A procedure has been also proposed to design an optimized array of independent primary coils for the ground station of a WPT charging system. Thanks to this approach, it is possible to mitigate the inconveniences produced by possible coil misalignment due to an imperfect landing of the drone.

Numerical and experimental results have been presented in terms of electrical performances to demonstrate the validity of the proposed WPT application. In particular, the proposed solution allows for the achievement of good electrical performances combined with an excellent tolerance to coil misalignment. This aspect is of fundamental importance for the automatic recharge of the drone battery. Finally, the proposed solution reduces the weight and size of the onboard WPT systems without altering the flight capabilities of the drone, maintaining almost unchanged the payload and the vision of the on-board apparatuses such as cameras and sensors.

Author Contributions: T.C., S.C., and M.F. conceived and planned the experiments. T.C. carried out the experiments. S.C. and M.F. planned and carried out the simulations. All authors provided critical feedback, improved the final design, analyzed the data and wrote the paper.

Conflicts of Interest: The authors declare no conflict of interest.

References

1. Sujit, P.B.; Ghose, D. Search using multiple UAVs with flight time constraints. *IEEE Trans. Aerosp. Electron. Syst.* **2004**, *40*, 491–509. [CrossRef]
2. Sarunic, P.; Evans, R. Hierarchical model predictive control of UAVs performing multitarget-multisensor tracking. *IEEE Trans. Aerosp. Electron. Syst.* **2014**, *50*, 2253–2268. [CrossRef]
3. Lee, B.; Kwon, S.; Park, P.; Kim, K. Active power management system for an unmanned aerial vehicle powered by solar cells, a fuel cell, and batteries. *IEEE Trans. Aerosp. Electron. Syst.* **2014**, *50*, 2253–2268. [CrossRef]
4. DIJ. Available online: https://www.dji.com/ (accessed on 14 September 2017).
5. Lee, D.; Zhou, J.; Lin, W.T. Autonomous battery swapping system for quadcopter. In Proceedings of the 2015 International Conference on Unmanned Aircraft Systems (ICUAS), Denver, CO, USA, 9–12 June 2015; pp. 118–124.
6. Knorr, S.; Puiatti, L.; Dallachiesa, M.; Puiatti, A. Charging Apparatus and Method for Electrically Charging Energy Storage Devices. Patent WO2015107199 A1, 23 July 2015.
7. Covic, G.A.; Boys, J.T. Inductive power transfer. *Proc. IEEE* **2013**, *101*, 1276–1289. [CrossRef]
8. Shinohara, N. Power without wires. *IEEE Microw. Mag.* **2011**, *11*, 64–73. [CrossRef]

9. Campi, T.; Cruciani, S.; Maradei, F.; Feliziani, M. Near Field reduction in a Wireless Power Transfer System using LCC compensation. *IEEE Trans. Electromagn. Compat.* **2017**, *59*, 686–694. [CrossRef]
10. Campi, T.; Cruciani, S.; De Santis, V.; Feliziani, M. EMF safety and thermal aspects in a pacemaker equipped with a wireless power transfer system working at low frequency. *IEEE Trans. Microw. Theory Tech.* **2016**, *64*, 375–382. [CrossRef]
11. Jawad, A.M.; Nordin, R.; Gharghan, S.K.; Jawad, H.M.; Ismail, M. Opportunities and Challenges for Near-Field Wireless Power Transfer: A Review. *Energies* **2017**, *10*, 1022. [CrossRef]
12. Vijayakumaran Nair, V.; Choi, J.R. An Efficiency Enhancement Technique for a Wireless Power Transmission System Based on a Multiple Coil Switching Technique. *Energies* **2016**, *9*, 156. [CrossRef]
13. Feliziani, M.; Campi, T.; Cruciani, S.; Maradei, F.; Grasselli, U.; Macellari, M.; Schirone, L. Robust LCC compensation in wireless power transfer with variable coupling factor due to coil misalignment. In Proceedings of the 2015 IEEE 15th International Conference on Environment and Electrical Engineering (EEEIC), Rome, Italy, 10–13 June 2015.
14. Campi, T.; Dionisi, F.; Cruciani, S.; De Santis, V.; Feliziani, M.; Maradei, F. Magnetic field levels in drones equipped with wireless power transfer technology. In Proceedings of the 2016 Asia-Pacific International Symposium on Electromagnetic Compatibility (APEMC), Shenzhen, China, 17–21 May 2016; pp. 544–547.
15. Junaid, A.B.; Konoiko, A.; Zweiri, Y.; Sahinkaya, M.N.; Seneviratne, L. Autonomous Wireless Self-Charging for Multi-Rotor Unmanned Aerial Vehicles. *Energies* **2017**, *10*, 803. [CrossRef]
16. Choi, C.H.; Jang, H.J.; Lim, S.G.; Lim, H.C.; Cho, S.H.; Gaponov, I. Automatic wireless drone charging station creating essential environment for continuous drone operation. In Proceedings of the 2016 International Conference on Control, Automation and Information Sciences (ICCAIS), Ansan, Korea, 26–29 October 2016; pp. 132–136.
17. He, X.; Bito, J.; Tentzeris, M.M. A drone-based wireless power transfer and communications platform. In Proceedings of the 2017 IEEE Wireless Power Transfer Conference (WPTC), Taipei, Taiwan, 10–12 May 2017; pp. 1–4.
18. Mostafa, T.M.; Muharam, A.; Hattori, R. Wireless battery charging system for drones via capacitive power transfer. In Proceedings of the 2017 IEEE PELS Workshop on Emerging Technologies: Wireless Power Transfer (WoW), Chongqing, China, 20–22 May 2017; pp. 1–6.
19. Simic, M.; Bil, M.; Vojisavljevic, V. Investigation in Wireless Power Transmission for UAV Charging. *Proc. Comput. Sci.* **2015**, *40*, 1846–1855. [CrossRef]
20. Cruciani, S.; Campi, T.; Feliziani, M.; Maradei, F. Optimum coil configuration of wireless power transfer system in presence of shields. In Proceedings of the 2015 IEEE International Symposium on Electromagnetic Compatibility (EMC), Dresden, Germany, 16–22 August 2015; pp. 720–725.
21. Campi, T.; Cruciani, S.; Feliziani, M. Magnetic shielding of Wireless Power Transfer systems. In Proceedings of the 2014 International Symposium on Electromagnetic Compatibility, (EMC'14/Tokyo), Tokyo, Japan, 12–16 May 2014.
22. COMSOL Multiphysics Software. Available online: http://www.comsol.com (accessed on October 2017).
23. Round Litz Datasheet. Available online: http://litzwire.com/nepdfs/Round_Litz_Catalog.pdf (accessed on 14 September 2017).
24. D'Amore, M.; De Santis, V.; Feliziani, M. Equivalent circuit modeling of frequency-selective surfaces based on nanostructured transparent thin films. *IEEE Trans. Magn.* **2012**, *48*, 703–706. [CrossRef]
25. Buccella, C.; Feliziani, M. A hybrid model to compute the effects of a direct lightning stroke on three-dimensional structures. *IEEE Trans. Magn.* **2003**, *39*, 1586–1589. [CrossRef]
26. Campi, T.; Cruciani, S.; Palandrani, F.; De Santis, V.; Hirata, A.; Feliziani, M. Wireless Power Transfer charging system for AIMDs and pacemakers. *IEEE Trans. Microw. Theory Tech.* **2016**, *64*, 633–642. [CrossRef]
27. Ghommam, J.; Saad, M. Autonomous Landing of a Quadrotor on a Moving Platform. *IEEE Trans. Aerosp. Electron. Syst.* **2017**, *53*, 1504–1519. [CrossRef]
28. Campi, T.; Cruciani, S.; Maradei, F.; Feliziani, M. High efficiency and lightweight wireless charging system for drone batteries. In Proceedings of the 2015 AEIT International Annual Conference (AEIT), Cagliari, Italy, 20–22 September 2017; pp. 1–5.
29. Zhang, W.; Mi, C.C. Compensation topologies of high-power Wireless Power Transfer systems. *IEEE Trans. Veh. Technol.* **2016**, *65*, 4768–4778. [CrossRef]

30. Liu, X.; Wang, T.; Yang, X.; Jin, N.; Tang, H. Analysis and Design of a Wireless Power Transfer System with Dual Active Bridges. *Energies* **2017**, *10*, 1588. [CrossRef]
31. Aldhaher, S.; Kkelis, D.; Yates, D.C.; Mitcheson, P.D. Class EF2 inverters for wireless power transfer applications. In Proceedings of the 2015 IEEE Wireless Power Transfer Conference (WPTC), Boulder, CO, USA, 13–15 May 2015; pp. 1–4.